

Structure-Based Drug Design of Novel Aurora Kinase A Inhibitors: Structural Basis for Potency and Specificity

Mohane Selvaraj Coumar,^{†,¶} Jiun-Shyang Leou,^{†,¶} Paritosh Shukla,[†] Jian-Sung Wu,[†] Ajay Kumar Dixit,[†] Wen-Hsing Lin,[†] Chun-Yu Chang,[†] Tzu-Wen Lien,[†] Uan-Kang Tan,[‡] Chun-Hwa Chen,[†] John T.-A. Hsu,[†] Yu-Sheng Chao,[†] Su-Ying Wu,^{*,†} and Hsing-Pang Hsieh^{*,†}

Division of Biotechnology and Pharmaceutical Research, National Health Research Institutes, 35 Keyan Road, Zhunan, Miaoli County 350, Taiwan, ROC, and Department of Chemical and Materials Engineering, Technology and Science Institute of Northern Taiwan, Taipei 112, Taiwan, ROC

Received October 7, 2008

Aurora kinases have emerged as attractive targets for the design of anticancer drugs. Through structure-based virtual screening, novel pyrazole hit **8a** was identified as Aurora kinase A inhibitor ($IC_{50} = 15.1 \mu M$). X-ray cocrystal structure of **8a** in complex with Aurora A protein revealed the C-4 position ethyl carboxylate side chain as a possible modification site for improving the potency. On the basis of this insight, bioisosteric replacement of the ester with amide linkage and changing the ethyl substituent to hydrophobic 3-acetamidophenyl ring led to the identification of **12w** with a ~ 450 -fold improved Aurora kinase A inhibition potency ($IC_{50} = 33 \text{ nM}$), compared to **8a**. Compound **12w** showed selective inhibition of Aurora A kinase over Aurora B/C, which might be due to the presence of a unique H-bond interaction between the 3-acetamido group and the Aurora A nonconserved Thr217 residue, which in Aurora B/C is Glu and found to sterically clash with the 3-acetamido group in modeling studies.

Introduction

Aurora kinases belong to serine/threonine subclass of kinases and are involved in the regulation of mitosis.¹ Three isoforms (A, B, and C) are known, which differ in their amino acid length and sequence at the N-terminal domain but have a conserved ATP binding site.² Aurora A is involved in centrosome maturation and separation, bipolar spindle assembly, and mitotic entry. While Aurora B is essential for accurate chromosome segregation and cytokinesis, Aurora C complements the function of Aurora B.¹ Aurora A and B levels both are up-regulated in various cancers, including breast and colorectal cancers;³ deregulated Aurora kinase activity has been linked to genetic instability, defects in centrosome function, spindle assembly, chromosome alignment, and cytokinesis, all of which can lead to tumorigenesis.¹ Hence, inhibition of Aurora kinase activity by targeting the ATP binding site with small molecules is emerging as a new anticancer target-based therapy. Moreover, in vivo studies with Aurora inhibitors **1** (MK-0457/VX-680),^{4,5} **2** (PHA-739358),^{6,7} **3** (MLN8054),⁸ and **4** (AZD1152)^{9,10} (Figure 1) in various animal models have shown tumor regression and are now in different stages of clinical development for various cancers.

Molecular targeted therapies, such as Aurora kinase inhibition, target cancer cells more specifically than traditional cancer treatment options, such as antimetabolic agents. Since Aurora kinase is emerging as a promising molecular drug target for cancer, we continued our efforts to find anticancer drugs¹¹ by developing a program to search for novel Aurora kinase inhibitors. Various research groups have reported different lead generation strategies for Aurora inhibitors, such as high

throughput screening (HTS^a), fragment-based screening, and synthetic modifications of known kinase core structures.^{6,12,13} However, only a few studies have reported virtual screening-based lead generation of modestly potent compounds and have not further demonstrated the utility of these lead compounds in generating potent Aurora kinase inhibitors.^{14,15} We, herein, report our virtual screening strategy, which led to the identification of a novel pyrazole lead compound **8a** (Aurora A $IC_{50} \approx 15 \mu M$), and the X-ray cocrystal structure-guided design for lead optimization, which culminated in the identification of **12w** (Aurora A $IC_{50} \approx 0.033 \mu M$) with a 450-fold improved Aurora kinase A inhibition compared to the lead **8a**. In addition **12w** showed selective Aurora A inhibition compared to Aurora B/C and also inhibited the cellular targets of Aurora kinase in the HCT-116 colon cancer cell line.

Lead Identification

The Aurora kinase structure^{6,12,16,17} represents a typical bilobal kinase fold containing the N-terminal β -strand domain and the C-terminal α -helix domain. The two domains are linked by a hinge region (residues 210–216), a loop forming the conserved hydrogen bonding interactions with the ATP or inhibitors, which is sandwiched between the two domains. The conserved H-bonding interactions of inhibitors with hinge region residues Glu211 and Ala213 are observed in most of the inhibitor–Aurora complex structures and are essential for maintaining activity. For the virtual screening, 59 488 compounds from the Maybridge database (Tintagel, Cornwall,

* To whom correspondence should be addressed. For S.-Y.W.: phone, +886-37-246-166, extension 35713; fax, +886-37-586-456; e-mail, slying@nhri.org.tw. For H.-P.H.: phone, +886-37-246-166, extension 35708; fax, +886-37-586-456, e-mail, hphsieh@nhri.org.tw.

[†] National Health Research Institutes.

[¶] These authors contributed equally to this work.

[‡] Technology and Science Institute of Northern Taiwan.

^a Abbreviations: CLogP, calculated logarithm of partition coefficient; EDC, 1-(3-dimethylaminopropyl)-3-ethylcarbodiimide; EPHA1, EPH receptor A1; HCT-116, human colon cancer-116 cell line; HOBt, 1-hydroxybenzotriazole; HTS, high throughput screening; JAK2, Janus-activated kinase 2; KIT, Hardy–Zuckerman 4 feline sarcoma viral oncogene homologue; LCMS, liquid chromatography coupled mass spectrometry; PDB ID, Protein Data Bank identification number; RET, Ret proto-oncogene; SBDD, structure-based drug design; TBST, Tris-buffered saline Tween-20; TPSA, total polar surface area; TRKA, neurotrophic tyrosine kinase receptor type 1; VEGFR, vascular endothelial growth factor receptor.

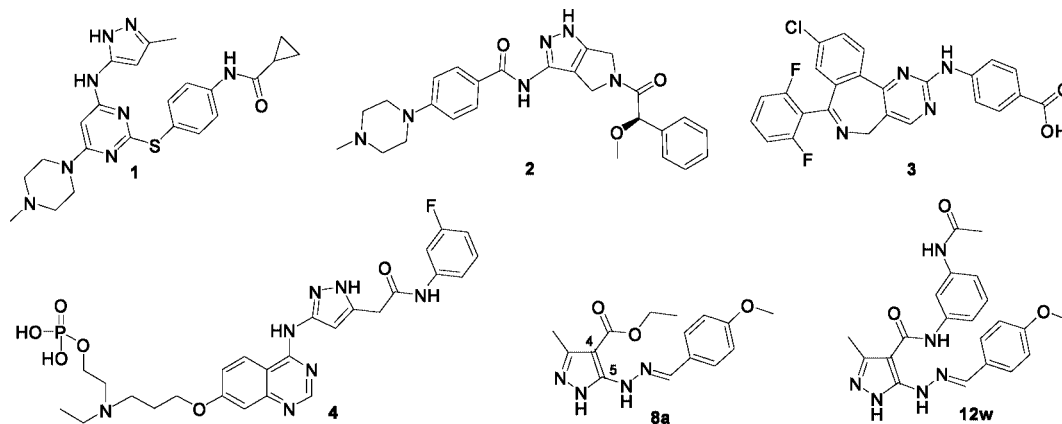


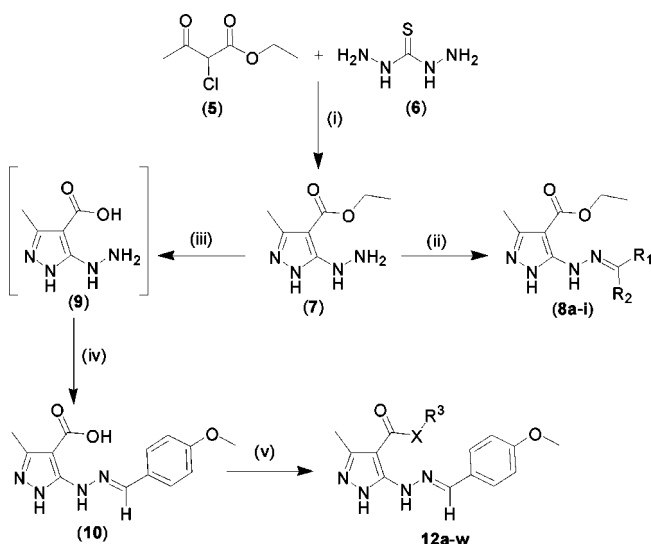
Figure 1. Aurora kinase inhibitors **1–4** in clinical testing as anticancer treatment. New compounds **8a** and **12w** identified in this study have a pyrazole ring in their scaffold, similar to compounds **1**, **2**, and **4**.

England) were docked into the binding site of Aurora kinase A by GOLD, version 3.1, using the crystal structure of Aurora kinase A in complex with ADP as the template (PDB ID 1OL5). H-Bonding interactions of inhibitors with the hinge region of Aurora kinase, including Glu211 and Ala213, are critical for the binding, as revealed by various Aurora kinase–inhibitor complex structures;^{4,6,12,16} consequently, H-bond constraints implemented in GOLD were applied in the docking experiment to specify that one or both of the hinge region residues, Glu211 and Ala213, should form an H-bond with the docked compound. The docked compounds were then ranked by Gold score, and the top-ranked 100 compounds were experimentally evaluated for their ability to inhibit Aurora kinase A activity. Among them, compounds with two different core structures showed >50% inhibition of Aurora kinase A activity when tested at 50 μ M concentration. Preliminary investigations of one of these, a tricyclic core structure, were recently reported by our laboratory.¹⁸ While three compounds shared a pyrazole core structure, **8a** (Figure 1), the most active of these has a *p*-methoxyphenylhydrazone group at the C-5 position. Literature studies revealed that even though substituted pyrazoles are a common feature of various kinase inhibitor scaffolds, the presence of phenylhydrazone moiety makes compound **8a** novel, which prompted us to further investigate its potential for Aurora inhibition.

Chemistry

The hit compound **8a** was synthesized using a modified literature method (Scheme 1).¹⁹ Condensation of 2-chloro-3-oxobutyrlic acid ethyl ester **5** with thiocarbonylhydrazide **6** in refluxing ethanol under acidic conditions led to one-step construction of the pyrazole ring **7** with the C-4 position ethyl carboxylate and C-5 position hydrazine function. The hydrazine functionality was further converted to the hydrazone by reacting with *p*-anisaldehyde in toluene under reflux condition using a Dean–Stark assembly to obtain the target compound **8a**, with a yield of 22% over two steps. Similarly, condensation of requisite aldehyde or ketone with **7** gave **8b–i**. In an attempt to modify the functional group at the C-4 position of the pyrazole ring, hydrolysis of the ethyl carboxylate group of **8a** to give the acid **10** using LiOH, NaOH, or KOH was carried out but was not successful because of the instability of the hydrazone in basic condition. We subsequently tried to hydrolyze the ester group before introducing the hydrazone moiety. Thus, when compound **7** was hydrolyzed with NaOH, the desired product **9** could be detected by LCMS, but attempts to isolate the product failed. The intermediate **9** was converted in

Scheme 1. Synthesis of Pyrazole Analogues^a



^a Reagents: (i) HCl, EtOH, reflux, 1 h, 27%; (ii) aldehyde/ketone, PhCH₃, reflux, 2 h, 40–83%; (iii) 1 N NaOH, H₂O–MeOH, 80 °C, 2 h; (iv) (a) neutralize to pH ~7; (b) *p*-anisaldehyde, CH₂Cl₂–MeOH, reflux, 2 h, 55% over two steps; (v) R³XH (**11**, amine, aniline, alcohol), HOBt, EDC, DMF, room temp, 24 h, 15–26%.

situ to the desired hydrazone **10** by reacting with *p*-anisaldehyde, which could be isolated from the reaction mixture as a solid product in 55% yield over two steps. After several attempts with various coupling agents for the final acid-amine/alcohol coupling step, we found that HOBt and EDC mediated coupling in DMF at room temperature gave **12a–w** with moderate yields (Scheme 1).

Results and Discussion

The lead compound **8a** identified through virtual screening showed IC₅₀ ≈ 15 μ M for Aurora kinase A enzyme inhibition in kinase-glo assay.¹⁸ Because of the availability of a range of aldehyde reagents and the synthetic accessibility, modifications at the 5-position of **8a** was taken up first for SAR studies (Table 1). It was found that when an electron-donating methoxy group was removed, the unsubstituted phenyl analogue **8b** showed a decreased Aurora kinase inhibition; the loss of activity, however, was much more pronounced when this phenyl group was replaced with a benzyl group (**8c**). When an electron-withdrawing substituent such as a fluoro group was introduced in the phenyl ring, the activity was retained in **8d**, but a bulky

Table 1. Physicochemical Properties and Inhibition of Aurora Kinase A by Pyrazoles **8a–i**

8a-i

Compound	R ¹	R ²	MW ^a	CLogP ^a	TPSA ^b	Aurora Kinase A Inhibition ^c	
						% Inhibition at 10 μ M	IC ₅₀ μ M
8a		H	302.33	3.64	88.613	33.9	15.140
8b		H	272.30	3.41	79.379	16.4	-
8c		H	286.33	3.27	79.379	3.6	-
8d		H	290.29	3.57	79.379	36.5	-
8e		H	348.40	5.30	79.379	27.5	-
8f		H	370.45	2.99	85.855	41.0	-
8g		H	311.34	3.76	95.17	50.0	11.505
8h		H	311.34	3.76	95.17	50.3	13.740
8i		CH ₃	316.36	4.13	88.613	18.2	-

^a MW and CLogP calculated using ChemDraw Ultra, version 7.0. ^b TPSA computed from www.molinspiration.com. ^c Values are expressed as the mean of at least two independent determinations and are within $\pm 15\%$.

hydrophobic phenyl substituent (**8e**) was a deterrent for the activity. On the other hand, introduction of a hydrophilic 4-methylpiperazine moiety (**8f**) on the phenyl ring was tolerated. When the phenyl ring was replaced with a 5- or 4-indolyl ring system (**8g,h**), the activity level slightly improved compared to **8a**. However, 3-, 6-, and 7-indolyl analogues were not better than **8a** (data not shown). Also, when the benzylidene H in **8a** ($R_2 = H$) was replaced with a methyl group in **8i** ($R_2 = CH_3$), the activity declined (later X-ray cocrystal of **8a**–Aurora A revealed that this methyl group might cause steric clash with Leu139 and Arg137).

Concurrent with our forementioned SAR studies to understand the binding mode and to get structural insights that could help in the design of more potent Aurora inhibitors, we cocrystallized **8a** with Aurora kinase A and solved the inhibitor–Aurora A protein complex structure. The electron density maps of Aurora kinase A in complex with **8a** are clear (Figure 2) except for some disordered regions that include residues 280–291 and 393–401. The activation loop residues 280–291 containing the T288D mutation are highly flexible in many published

structures.^{6,12,16} The complex structure revealed that the compound **8a** binds to Aurora kinase A in the ATP-binding site located in the cleft between the two domains. The pyrazole ring of **8a** fitted into the hinge region, and the pyrazole ring N2 and N1H atoms formed two H-bonds (2.92 Å and 3.03 Å) with the main chain of Ala213. Similar H-bond interactions between the ligand and hinge region residues of Aurora kinase were conserved in most Aurora inhibitor complex structures and are important for the inhibitor binding.^{4,6} In addition, the pyrazole ring also formed hydrophobic interactions with the surrounding residues, including Leu139, Val147, Ala160, and Leu263. Particularly, Leu263 made extensive interactions with the pyrazole ring. The C-5 position *p*-methoxyphenyl group of **8a** extended into the solvent-exposed region of the binding site and had hydrophobic interactions with Gly216 and Pro214, while the hydrazonide group ($-NH-N=CH-$) that served as a linker between the pyrazole and *p*-methoxyphenyl group made few interactions (only with Gly216). The C-4 position ethyl carboxylate group was situated under the p-loop and had close contact with protein residues, such as Gly140, Val147, and

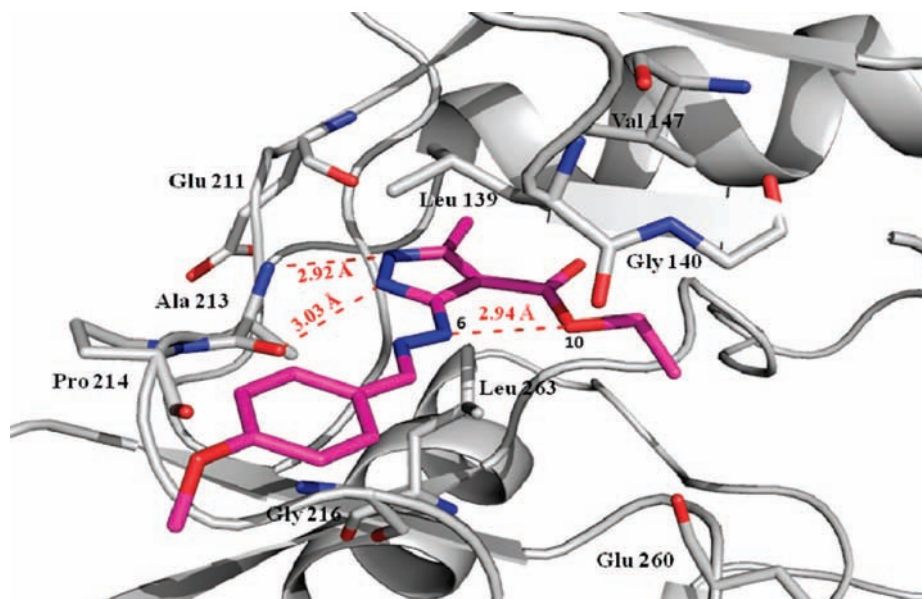


Figure 2. X-ray cocrystal structure of **8a** in complex with Aurora A. Compound **8a** binds to the ATP-binding pocket of Aurora A through two H-bond interactions with hinge Ala213 residue. An intramolecular H-bond between the two side chains of **8a** is seen, resulting in pseudobicyclic conformation of the molecule. The 4-methoxy group projects to the solvent exposed part, and the ester function of **8a** is projected into a hydrophobic pocket of Aurora A.

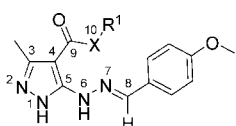
Thr217. Furthermore, the ethyl carboxylate group is adjacent to a hydrophobic region consisting of Leu139, Gly140, Val147, Thr217, Glu260, and Leu263. Finally, it is worth noting that **8a** adopts a conformation to form an intramolecular H-bond (2.94 Å) between the two side chains at position C-4 and C-5, through N6H in the hydrazone group ($-\text{NH}-\text{N}=\text{CH}-$) and O10 in the ethyl carboxylate ($-\text{OC}_2\text{H}_5$) group, thereby forming a pseudobicyclic ring structure when bound to Aurora A protein.

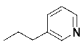
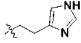
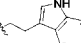
On the basis of our findings from the X-ray structure (that the C-5 position hydrazone substituent of the molecule is projected into the solvent accessible part of the Aurora protein, while the 4-position ethyl carboxylate functionality is projected into a possible hydrophobic portion of the Aurora kinase protein), we envisaged that functional modification of the ethyl carboxylate at the C-4 position of the pyrazole could lead to enhanced activity. In addition, the limited success in improving the activity of the lead **8a** by modifying the C-5 position hydrazone part prompted us to focus our efforts on replacing the C-4 position ethyl group with a hydrophobic phenyl ring, which would provide additional hydrophobic interactions between the ligand and the protein and could enhance the potency. Thus, in an attempt to increase the hydrophobic interaction between the ligand and Aurora kinase, benzyl carboxylate **12a** was synthesized; as envisaged, this showed a 3-fold increase in Aurora inhibitory activity compared to ethyl carboxylate **8a** (Table 2). Next, by utilization of the concepts of bioisosterism, the ester linkage of **12a** was replaced with the amide linkage to give **12b**. Conversion of the C-4 position ester to the amide linkage led to another 3-fold improvement in activity for **12b** ($\text{X} = \text{NH}$) compared to **12a** ($\text{X} = \text{O}$). To examine the role of bioisosteric replacement of O with NH in enhancing the potency and to understand the difference in the molecular level interaction between the ligand and Aurora kinase protein, the X-ray cocrystal structures of **12a** and **12b** were solved.

Comparison of the cocrystal structure of **12a** with **8a** reveals that the pyrazole ring, hydrazone linker, and *p*-methoxyphenyl groups of these two compounds superimpose well. The additional phenyl ring of **12a** in the C-4 position sandwiched itself between the p-loop and the hydrophobic region, and it made

extra hydrophobic interactions with Gly140, Thr217, and Glu260. The additional hydrophobic interactions contributed to the improved potency of **12a** compared to **8a**. Overall, both **8a** and **12a** have similar conformation when bound to Aurora kinase and formed pseudobicyclic structures through intramolecular H-bonding. In contrast, comparison of **12b** and **12a** (Figure 3) revealed that although these are bioisosteric with only one atom difference (NH vs O), **12b** adopts a different conformation and has a different three-dimensional spatial arrangement when bound to Aurora A (Figure 3). The pyrazole ring of **12b** moved closer to Glu211, which led to the formation of an H-bond with the carbonyl O of Glu211 (2.84 Å) and another H-bond with the backbone NH of Ala213 (2.70 Å). The shift of the pyrazole ring in **12b** consequently moved the hydrazone linker close to the Ala213 and allowed a third H-bond formation between the hydrazone N6H and carbonyl O of Ala213 (2.84 Å). Therefore, **12b** has three H-bonds with the hinge region while, similar to **8a**, **12a** formed only two H-bonds with the hinge region.

Moreover, the torsion angle of $-\text{N1}-\text{C5}-\text{N6}-\text{N7}=\text{moiety}$ rotated from -11.8° (in **12a** structure) to -164.8° (in **12b** structure), which led to different intramolecular H-bonding patterns between the two side chains of both compounds. In the structure of **12b**, the N7 atom of hydrazone linker formed an intramolecular H-bond with the amide N10H (2.87 Å), while in the structure of **12a** the N6H of hydrazone formed an intramolecular H-bond with the ester O10 (3.0 Å). Also, in **12b** the intramolecular H-bond generated a pseudobicyclic structure and likely stabilized the orientation of the pyrazole ring, which would contribute to its interactions with the protein. Notably, the N6H of the hydrazone group played a different role in these two structures. It provided an external H-bond with the hinge residue of the protein in the complex structure of **12b** with Aurora A, while it provided an intramolecular H-bond within the compound in the structure of **12a** and had no interactions with the protein. Finally, the phenyl ring of **12b** orientated differently from that of **12a** and made additional interactions with Glu260 and Leu263; this, along with the additional H-bonding with the hinge region, contributed to the improved activity of **12b** compared to **12a**. Thus, bioisosteric replacement

Table 2. Physicochemical Properties and Inhibition of Aurora Kinase A by Pyrazoles **8a** and **12a–w**


Compounds	X	R ¹	MW ^a	CLogP ^a	TPSA ^b	Aurora Kinase A Inhibition IC ₅₀ (μM) ^c
8a	-O-	-CH ₂ CH ₃	302.33	3.64	88.613	15.140
12a	-O-	-CH ₂ Ph	364.40	4.94	88.613	5.250
12b	-NH-	-CH ₂ Ph	363.41	3.55	91.406	1.580
12c	-NH-	-CH ₂ CH ₂ Ph	377.44	3.68	91.406	1.350
12d	-NH-	-CH ₂ CH ₂ CH ₂ Ph	391.47	4.06	91.406	1.942
12e	-NH-	-Ph	349.39	3.37	91.406	0.804
12f	-NCH ₃	-Ph	363.41	3.44	82.617	> 50
12g	-NCH ₃	-CH ₂ Ph	377.44	3.86	82.617	> 50
12h	-NH-		378.43	2.18	104.298	1.484
12i	-NH-		367.41	1.28	120.089	1.937
12j	-NH-		416.48	3.67	107.197	1.071
12k	-NH-	-CH ₂ (Ph-4-OCH ₃)	393.44	3.47	100.64	1.623
12l	-NH-	-CH ₂ (Ph-3-OCH ₃)	393.44	3.47	100.64	0.838
12m	-NH-	-CH ₂ (Ph-3-NHCOCH ₃)	420.46	2.57	120.504	1.746
12n	-NH-	-CH ₂ CH ₂ (Ph-4-OCH ₃)	407.47	3.60	100.64	1.580
12o	-NH-	-CH ₂ CH ₂ (Ph-3-OCH ₃)	407.47	3.60	100.64	2.895
12p	-NH-	-Ph-4-OCH ₃	379.41	3.35	100.64	0.460
12q	-NH-	-Ph-3-OCH ₃	379.41	3.35	100.64	0.449
12r	-NH-	-Ph-2-OCH ₃	379.41	2.76	100.64	1.087
12s	-NH-	-Ph-3,4-di-OCH ₃	409.44	2.99	109.874	0.960
12t	-NH-	-Ph-4-N(CH ₃) ₂	392.45	3.54	94.644	1.568
12u	-NH-	-Ph-4-F	367.38	3.61	91.406	1.447
12v	-NH-	-Ph-4-NHCOCH ₃	406.44	2.39	120.504	0.719
12w	-NH-	-Ph-3-NHCOCH ₃	406.44	2.39	120.504	0.033 ^d

^a MW and CLogP calculated using ChemDraw Ultra, version 7.0. ^b TPSA computed from www.molinspiration.com. ^c Values are expressed as the mean of at least two independent determinations and are within ±15%. ^d Values are expressed as the mean of four independent determinations and are within ±15%.

of O with NH had resulted in altering both the intramolecular and intermolecular interactions because of the difference in their ability to act as a hydrogen bond donor and/or acceptor groups.

Following the important observation that the intramolecular H-bonding network is different for ester linked compound **12a** and amide linked compound **12b** in protein bound conformation, we investigated the effect of the length of the alkyl chain connecting the phenyl ring to the amide bond in **12b**. Increasing the chain length as in **12c,d** did not alter the activity level much in comparison to **12b**. When the phenyl ring was directly linked to the amide bond in **12e**, however, the Aurora inhibition reached the highest level. To rationalize these structure–activity

relationship trends, we also solved the X-ray cocrystal structures of **12c–e**. Superimposition of the X-ray cocrystal structures of **12b–e** revealed that the intramolecular H-bonding network, hinge interacting residues, and the interaction of the C-5 position hydrazone side chain are the same. All four compounds adopt very similar conformations except for the phenyl rings in the C-4 position carboxamide side chain. The phenyl ring of **12c** and **12e** moved closer to the p-loop and interacted with the surrounding residues (for example, Leu139, Gly140, and Leu141), whereas the phenyl ring of **12b** and **12d** rotated 90° and shifted away from the p-loop (Figure 4). The close interaction of the phenyl ring of **12e** with the p-loop might have

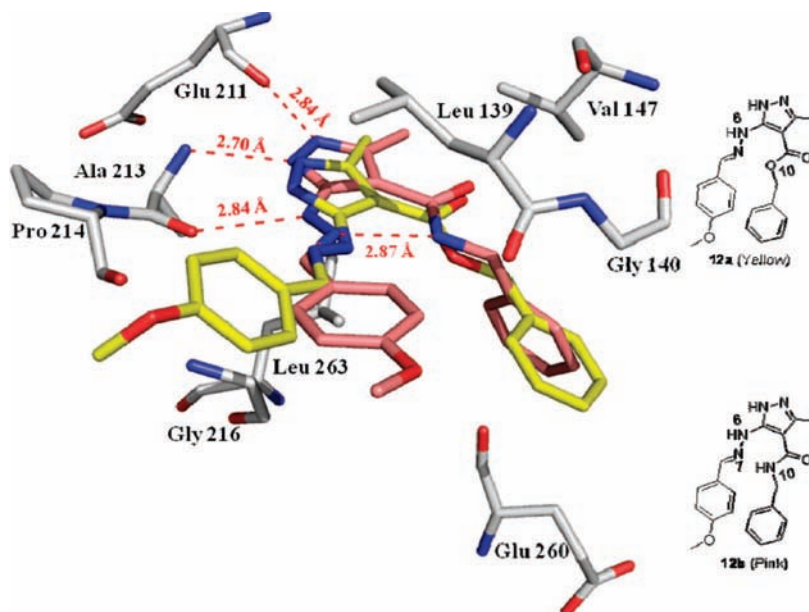


Figure 3. Comparison of X-ray cocrystal structures of **12a** (yellow) and **12b** (pink) in complex with Aurora A. Both the intra- and intermolecular H-bonding patterns are different when **12a** (X = O) is converted to **12b** (X = NH). Compared to **12a**, **12b** forms an additional H-bond interaction with the hinge Glu211 residue of Aurora A, resulting in enhanced potency for **12b**.

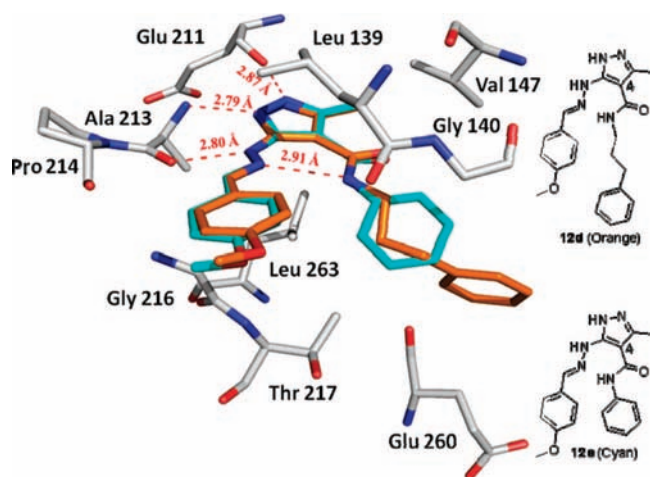


Figure 4. Comparison of X-ray cocrystal structures of **12d** (orange) and **12e** (cyan) in complex with Aurora A. The C-4 position phenyl ring in **12e** is closer and makes extra hydrophobic contacts with the p-loop, compared to **12d**.

stabilized the p-loop and consequently led to the improved potency of this compound. The X-ray cocrystal structure of **8a** and **12a–e** reveals that changing the ester (**8a**, **12a**) to the amide group (**12b–e**) resulted in a change in the intramolecular hydrogen bonding pattern and provided additional H-bond interactions with the hinge region of the Aurora kinase. Moreover, compounds **12b–e** had additional hydrophobic interaction with the Aurora kinase through the C-4 position phenyl rings, all of which contributed to the enhanced activity.

The presence of pseudobicyclic ring through intramolecular hydrogen bonding in all six cocrystals that were solved prompted us to investigate the importance of this molecular feature for Aurora kinase activity. Hence, the disubstituted amide **12f** was synthesized, which through interference of the *N*-CH₃ group would impede the pseudobicyclic ring formation through hydrogen bonding between the two side chains at the C-4 and C-5 positions. Compound **12f** (IC₅₀ > 50 μM) was found to be inactive when compared to **12e** (IC₅₀ = 0.8 μM), revealing that

for this class of compounds the ability to adopt a pseudobicyclic ring conformation through intramolecular H-bonding when bound to Aurora protein is essential for maintaining Aurora kinase activity. Similarly, the *N*-CH₃ analogue **12g** was also inactive, which further validates this observation. Even though intramolecular H-bond leading to pseudobicyclic ring structures has been documented in other ligands, such as VEGFR inhibitors,²⁰ the presence of distinct intramolecular H-bonding network in bioisosterically related compounds (**12a** and **12b**) leading to the formation of pseudobicyclic ring conformation is unique.

X-ray cocrystals of **12b,c,e** reveal that the C-4 position side chain phenyl group is surrounded closely by amino acid residues, e.g., Thr271, Asn261, and Glu160. This prompted us to investigate the effect of ring variations and aromatic ring substitutions, which could possibly form additional hydrogen bonding interactions with the Aurora protein and thus might lead to an enhancement in potency. To this end, we studied heteroaromatic systems, such as pyridine (**12h**), imidazole (**12i**), and indole (**12j**), which have the potential to form hydrogen bonding interaction by acting as a hydrogen donor or acceptor system. None of these compounds (**12h–j**), however, were superior to the corresponding phenyl compound, **12c**. Having found that compound **12e** has the optimal activity for further SAR studies and also noting that a large array of substituted anilines, benzylamines, and phenylethylamines are commercially available for investigation, we carried out focused SAR studies on three compounds: **12b,c,e**. In the benzylamine series introduction of either 4-methoxy (**12k**) or 3-acetamido (**12m**) function did not result in improvement in potency compared to the unsubstituted compound, **12b**. When a 3-methoxy (**12l**) group was introduced, however, a 2-fold improvement of activity was realized. Introduction of other functionalities, such as 4-F and the 4-NH₂ group, did not alter the activity level (data not shown) compared to the unsubstituted compound. SAR studies in the phenylethylamine series revealed that, similar to the situation with the benzylamine series, introduction of 4-methoxy (**12n**) or 3-methoxy (**12o**) has no advantage over the unsubstituted compound, **12c**. Other functional groups (such as 4-F,

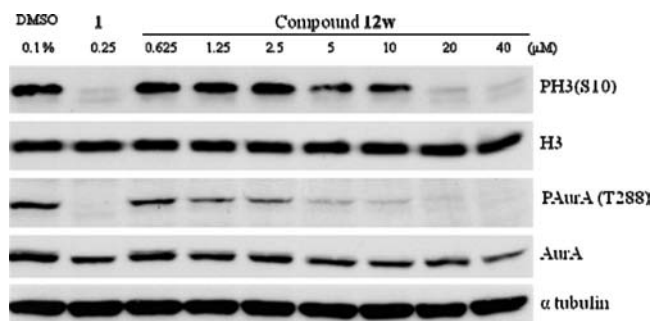


Figure 5. Western blotting analysis for cellular target modulation by **12w** inhibitor. Compound **12w** inhibits both phospho Aurora A (T288) and phospho histone H3 (Ser10) formation in HCT-116 cells.

4-OH, and 4-SO₂NH₂) were also found to be ineffective in improving the potency when compared to the unsubstituted compound (data not shown).

Since attempts to improve the potency in benzylamine and phenylethylamine series (**12b** and **12c**, respectively) by aromatic ring substitution showed less success, we turned our attention to the effect of aromatic ring substitution in aniline series **12e**. Introduction of electron-donating substitution, such as methoxy in either para- (**12p**) or meta-position (**12q**), led to a 2-fold improvement in potency (IC₅₀ ≈ 450 nM) compared to the unsubstituted compound **12e** (IC₅₀ = 804 nM). However, methoxy substitution in ortho-position (**12r**) or 3,4-dimethoxy (**12s**) or 4-N(CH₃)₂ (**12t**) substitution showed no advantage over the unsubstituted **12e**. Also, introduction of electron-withdrawing groups such as 4-fluoro (**12u**) and 4-acetamido (**12v**) was not found to improve the Aurora inhibition of the unsubstituted **12e**. Subsequently, the acetamido function was moved from para to meta position; the resulting 3-acetamido compound, **12w**, showed a dramatic improvement in potency for Aurora A inhibition (IC₅₀ = 33 nM), which is approximately 450-fold better than the initial lead, **8a** (IC₅₀ = 15.1 μM).

Having identified a potent Aurora kinase A inhibitor, **12w**, through X-ray cocrystal guided lead optimization, we were interested to see the biochemical outcome of Aurora kinase inhibition at the cellular level using this novel inhibitor. At the cellular level, it is known that Aurora A undergoes autophosphorylation at Thr288 residue and decreased levels of phospho-Aurora A (Thr288) are observed after treatment with Aurora A selective inhibitor **3**.⁸ Histone H3 (Ser10) is known to be a substrate of Aurora B, and inhibition of Aurora B kinase activity has been shown to decrease the levels of phosphorylated H3 Histone (ser10) in HCT-116 cells. Thus, the level of histone H3 phosphorylation is considered a useful biomarker to evaluate the effect of Aurora kinase inhibitors in both preclinical and clinical settings.²¹ Since modulation of Aurora A (Thr288) and histone H3 (Ser10) phosphorylation levels could act as a useful biochemical marker to evaluate the Aurora kinase A and B inhibition at the cellular level, we treated the HCT-116 colon cancer cell line, which is sensitive to Aurora inhibition, with different concentrations of **12w** and analyzed the phosphorylated Aurora A (Thr288) and phosphorylated histone H3 (Ser10) protein contents using Western blotting analysis (Figure 5). Treatment of the HCT-116 cell line with **12w** resulted in lower levels of both phosphorylated histone H3 (Ser10) and phosphorylated Aurora A (Thr288) in a dose-dependent manner. Even though the concentration required to achieve this inhibition is in the micromolar range, it is important to note that the levels of inhibition of phosphorylated Aurora A (Thr288) and phosphorylated histone H3 (Ser10) are different; for example, Aurora

Table 3. Kinase Profiling of **12w**^a

kinase tested ^b	% inhibition at 1 μM
ABL1	17
AKT1 (PKB α)	13
ALK	1
AMPK A1/B1/G1	31
AURKA (Aurora A)	91
AURKB (Aurora B)	36
AURKC (Aurora C)	45
CDK2/cyclin A	48
CHEK1 (CHK1)	21
EGFR (ErbB1)	8
EPHA1	51
ERBB2 (HER2)	26
FLT1 (VEGFR1)	27
FLT3	48
FRAP1 (mTOR)	-6
IGF1R	11
IKBKE (IKK ε)	-8
JAK2 JH1 JH2	56
KIT	61
MAP2K1 (MEK1)	-14
MAPK14 (p38 α)	19
MET (cMet)	19
NTRK1 (TRKA)	66
PDK1	17
PLK1	11
RAF1 (cRAF) Y340D Y341D	-1
RET	76
SRC	33
TEK (Tie2)	4
PIK3CG (p110 γ)	-3
GSK3B (GSK3 β)	32

^a Carried out by Invitrogen. ^b Table abbreviations: ABL1, c-abl oncogene 1 receptor tyrosine kinase; AKT1, v-akt murine thymoma viral oncogene homologue 1; ALK, anaplastic lymphoma kinase; AMPK, protein kinase, AMP-activated β 1 noncatalytic subunit; CDK2, cyclin-dependent kinase 2; CHEK1 (CHK1), CHK1 checkpoint kinase; EGFR, epidermal growth factor receptor; EPHA1, EPH receptor A1; ERBB2, V-erb-b2 erythroblastic leukemia viral oncogene homologue 2; FLT1, Fms-related tyrosine kinase 1; FLT3, Fms-like tyrosine kinase 3; IGF1R, insulin-like growth factor I receptor; IKBKE (IKK ε), inhibitor of κ light polypeptide gene enhancer in B-cells, kinase ε; JAK2, Janus-activated kinase 2; KIT, Hardy-Zuckerman 4 feline sarcoma viral oncogene homologue; MAP2K1 (MEK1), mitogen-activated protein kinase kinase 1; MAPK14 (p38 α), mitogen-activated protein kinase 14; MET (cMet), met proto-oncogene; NTRK1 (TRKA), neurotrophic tyrosine kinase receptor type 1; PDK1, 3-phosphoinositide-dependent protein kinase; PLK1, polo-like kinase; RAF1 (cRAF), v-raf-leukemia viral oncogene 1; RET, ret proto-oncogene; SRC, Rous sarcoma oncogene cellular homologue; TEK (Tie2), TEK tyrosine kinase, endothelial; PIK3CG (p110 γ), phosphoinositide-3-kinase catalytic γ polypeptide; GSK3B (GSK3 β), glycogen synthase kinase 3 β.

A showed more inhibition than Aurora B at 1.25, 2.5, 5, and 10 μM of **12w**, indicating that **12w** might be a selective inhibitor of Aurora A.

To confirm Aurora A selective inhibition by **12w** and also to know the selectivity over other kinases, we profiled **12w** over a panel of 30 therapeutically important kinases, including all three Aurora kinases (Table 3). Compound **12w** was tested for its ability to inhibit these kinases at 1 μM concentration; the results showed that **12w** indeed inhibits Aurora A better than all other kinases tested. Compared to Aurora A (91% inhibition at 1 μM), Aurora B (36%), and Aurora C (45%), kinase inhibition levels were lower, supporting the observation made in the Western blotting analysis that **12w** is a potent Aurora A subtype selective inhibitor. Among the other kinases profiled, all kinases showed <50% inhibition at 1 μM except for the following five kinases: RET (76%), TRKA (66%), KIT (61%), JAK2 (56%), and EPHA1 (51%). Because aberrant signaling of these kinases has been reported in various cancers, their inhibition might be an advantage and targeting them could lead to novel cancer treatment.

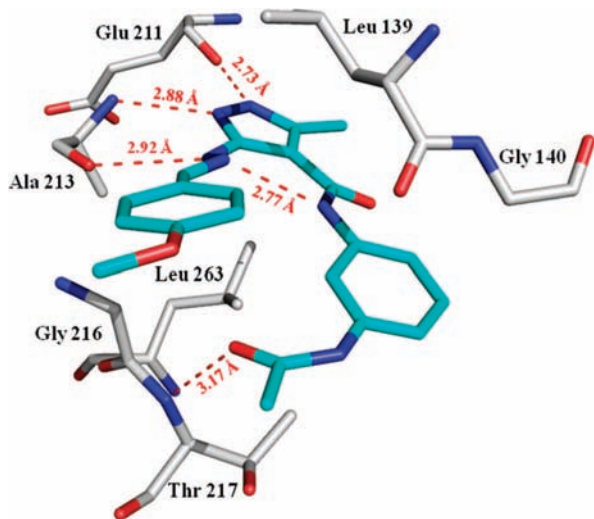


Figure 6. X-ray cocrystal structure of **12w** in complex with Aurora A. Compound **12w** binds to the ATP-binding pocket of Aurora A through four H-bond interactions, three with hinge Ala213 and Glu211 residues, and one with nonconserved Thr217 residue (PDB ID 3FDN).

Since introduction of the 3-acetamido group in **12e** led to a 25-fold improvement in activity for **12w** vs **12e**, we sought to understand the significance of the 3-acetamido group in enhancing the Aurora A inhibitory activity via solving the X-ray cocrystal structure of **12w** with Aurora A (Figure 6, PDB ID 3FDN). Superimposition of **12e** and **12w** revealed that the most significant difference between the two structures is that the 3-acetamido group is positioned near where the hinge loop is connected to the C-terminal lobe and forms H-bond interactions with Thr217. The O atom of the 3-acetamido group in **12w** is hydrogen-bonded with the main chain NH of Thr217 with a distance of 3.17 Å. The hydrogen bond with Thr217 is a unique feature of the **12w** cocrystal structures, as it is absent in all other available Aurora kinase–inhibitor complex structures. It is interesting to note that the Thr217 is a nonconserved residue in the active site of Aurora kinase, which is Thr217 in Aurora A and Glu in both Aurora B and Aurora C. Structural alignment of the **12w**–Aurora A complex structure with Aurora B (PDB ID 2VGP) showed that the 3-acetamido group of **12w** had a steric clash with the corresponding amino acid residue Glu177 in Aurora B (Figure 7), which could be the reason for the observed selectivity of **12w** for Aurora A kinase over Aurora B/C.

In addition to this extra hydrogen bond interaction with the Aurora A protein, the methyl group of 3-acetamido group has close contacts with Thr217 and Arg220. Moreover, in **12w** it was observed that the C-4 position side chain of pyrazole ring moved closer to the C-5 position hydrazone linker and formed a stronger intramolecular H-bond between the N7 and N10H atoms with a shorter distance of 2.77 Å, while in the case of **12e** the intramolecular H-bond distance was 2.91 Å. The stronger intramolecular H-bond interactions might better stabilize the pseudobicyclic conformation and contribute to the improved potency of **12w**.

With the X-ray cocrystal of **12w** in hand, we were interested to know how the molecular level interaction of this inhibitor compared with a known Aurora kinase inhibitor, which could help in designing better inhibitors in the future. Out of the four compounds that are in phase I/II clinical trials (**1**–**4**), the X-ray cocrystal structures of compounds **1**⁴ and **2**⁶ are disclosed. Both **1** and **2** have a common pyrazole ring in their respective

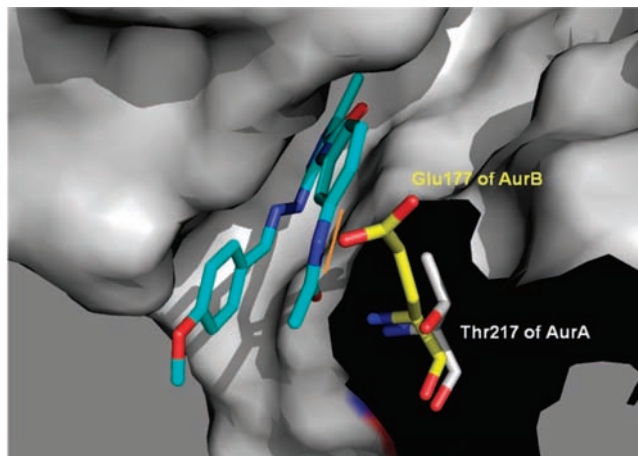


Figure 7. Molecular determinants for compound **12w**'s selectivity to Aurora A. Shown is the overlay of Aurora A–compound **12w** complex structure with Aurora B (PDB ID 2VGP). Glu177 of Aurora B would cause a steric clash with the 3-acetamido group in compound **12w**, indicated by the orange line.

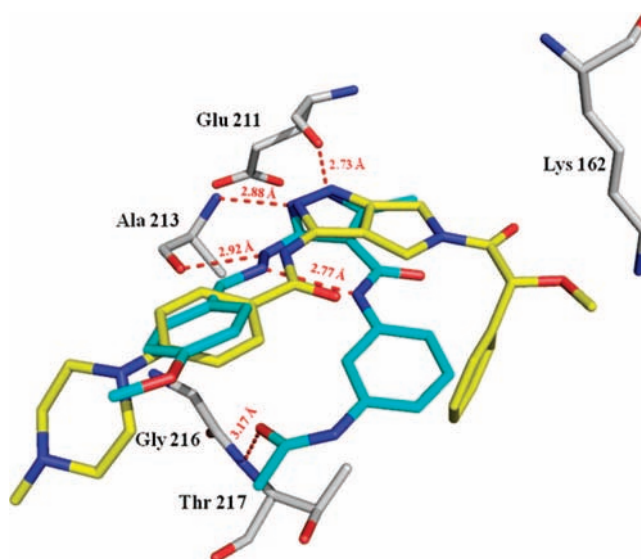


Figure 8. Comparison of X-ray cocrystal structures of **12w** (cyan) and **2** (yellow) in complex with Aurora A. Compound **12w** forms an H-bond with nonconserved Thr217 residue of Aurora A, which is absent in compound **2**.

structures, which forms an H-bond interaction with the hinge residue. We compared the X-ray cocrystal structure of **12w** with **2** (Figure 8), which is in phase II clinical trials and reported to be a potent pan-Aurora inhibitor with multikinase binding properties. Overlapping the two X-ray structures revealed that the pyrazole ring of **12w** superimposed well with the pyrazole ring of the tetrahydropyrrolopyrazole bicyclic core of **2** to form the conserved H-bonds with the Glu211 and Ala213. The 4-methoxyphenyl group of **12w** and the *N*-methylpiperazine group of **2** both extended to the solvent-exposed region of Aurora A. The major difference occurred in the orientation of the C4-position side chain bearing the 3-acetamido moiety in **12w**, which adopted a spatial position different from that of the phenylacetamide group of **2**. The 3-acetamido moiety of **12w** was directed toward the hinge loop adjacent to the C-terminal lobe and made the H-bonding interactions with Thr217, while the phenylacetamide group of **2** was close to the p-loop, and the OCH₃ group formed the H-bonding interactions with Lys162. The H-bond interactions with Lys162 contributed

significantly to the activity of **2**.⁶ In the case of **12w** bound with Aurora A, the distance of the carbonyl oxygen to the amino nitrogen of Lys162 is 6.61 Å, which is too far for H-bonding interactions. However, **12w** formed additional H-bond interactions with Thr217, which greatly contributed to the improved activity, as discussed in the previous section, and may compensate for the absence of the H-bonding interactions with Lys162.

Conclusion

Targeting Aurora kinases with novel small molecular inhibitors is gaining momentum as several inhibitors are undergoing clinical trials for cancer therapy. We have identified novel pyrazole analogue **8a** through structure-based virtual screening as an Aurora kinase A inhibitor. Structural insights obtained through X-ray cocrystal studies of **8a** suggested that modification of the C-4 position ethyl carboxylate side chain would improve potency. Bioisosteric replacement of the ester with amide linkage and changing the ethyl substituent to 3-acetamidophenyl led to the identification of **12w**, with a 450-fold improvement in Aurora A inhibition compared to **8a**. Different intramolecular H-bonding patterns in the X-ray cocrystal structure of the lead **8a** and **12w** were observed between the C-4 and C-5 position side chains, which locked the molecules in a pseudobicyclic conformation when bound to Aurora kinase A. The ability of this series of compounds to adapt to a pseudobicyclic ring conformation through intramolecular H-bonding is essential for demonstrating potent Aurora kinase activity. This information may provide a new insight in designing Aurora kinase inhibitors with a fused bicyclic system to mimic the pseudobicyclic ring conformation adapted by **12w**. Moreover, because of the different intramolecular H-bonding pattern observed in **8a** and **12w**, there was a change in the conformation/torsion angle of **12w**, leading to an additional H-bond formation with the hinge residue for **12w**. This additional H-bond interaction with the hinge residue, along with the H-bond interaction of 3-acetamido group with Thr217 and hydrophobic interactions provided by the phenyl group, contributed to the 450-fold enhancement in activity for **12w** compared to **8a**. The hydrogen bond with Thr217 is not present in any other reported Aurora kinase-inhibitor complex structure other than the **12w** cocrystal structure. Most interestingly, H-bond interaction of **12w** with the nonconserved residue Thr217 of Aurora A might have resulted in selective inhibition of Aurora A over Aurora B/C. Development of Aurora A or B/C specific inhibitors is useful in probing the importance of selective inhibition with respect to tumor development and treatment.

Experimental Section

General methods. All commercial chemicals and solvents are reagent grade and were used without further treatment unless otherwise noted. All reactions were carried out under an atmosphere of dry nitrogen. Reactions were monitored by TLC using Merck 60 F₂₅₄ silica gel glass backed plates (5 × 10 cm); zones were detected visually under ultraviolet irradiation (254 nm) or by spraying with phosphomolybdic acid reagent (Aldrich) followed by heating at 80 °C. Flash column chromatography was done using silica gel (Merck Kieselgel 60, no. 9385, 230–400 mesh ASTM). For small quantity purification, preparative TLC was carried out on precoated aluminum sheets (Merck no. 1.05554.0001, silica gel 60 F₂₅₄, 0.2 mm × 20 cm × 20 cm). ¹H NMR spectra were obtained with a Varian Mercury-300 spectrometer operating at 300 MHz. Chemical shifts were recorded in parts per million (ppm, δ) and were reported relative to the solvent peak or TMS. High-resolution mass spectra (HRMS) were measured with a Finnigan (MAT-95XL)

electron impact (EI) mass spectrometer. LCMS data were measured on an Agilent MSD-1100 ESI-MS/MS system.

Ethyl 5-Hydrazinyl-3-methyl-1H-pyrazole-4-carboxylate (7). To a stirred suspension of thiocarbonylhydrazide (**6**) (15.9 g, 150.0 mmol) in refluxing ethanol (150 mL) was added gradually concentrated HCl (50.0 mL) during 30 min, followed by dropwise addition of ethyl 2-chloroacetoacetate (**5**) (24.7 g, 20.7 mL, 150.0 mmol) during 30 min. The mixture was refluxed for a further 2 h and then brought to 10 °C by stirring over an ice bath for 15 min. The reaction mixture turned into a thick red mass, which was filtered on a G-3 sintered funnel. The residue was washed with cold ethanol (25 mL × 2). The yellow residue was dissolved in 60 mL of boiling water and then filtered to remove the sulfur impurities. The filtrate was neutralized on an ice bath to pH ~7.0 using 5 N aqueous NaOH solution. The neutral aqueous solution was extracted with *n*-BuOH (50 mL × 3). The *n*-BuOH layers were combined, washed with water (20 mL × 1), dried (MgSO₄), and evaporated to obtain the residue. This residue was dissolved in a mixture of methanol/CH₂Cl₂ (1:1, 100 mL) and filtered; the filtrate was evaporated and dried to obtain a yellowish-white amorphous powder of **7** (7.4 g, 27%). ¹H NMR (CDCl₃): δ 4.26 (q, *J* = 6.9 Hz, 2H), 2.39 (s, 3H), 1.34 (t, *J* = 7.1 Hz, 3H). LCMS-ESI (*m/z*): [M + 1]⁺ 185.1, [M + Na]⁺ 207.1.

(E)-Ethyl 5-(2-(4-Methoxybenzylidene)hydrazinyl)-3-methyl-1H-pyrazole-4-carboxylate (8a). Compound **7** (0.028 g, 0.15 mmol) and *p*-anisaldehyde (0.023 g, 0.17 mmol) in freshly dried toluene were refluxed for 2 h using a Dean-Stark assembly. Completion of reaction was monitored by TLC. The reaction mixture was evaporated, and the residue was subjected to preparative TLC using CH₂Cl₂/MeOH (98:2) to give **8a** (0.038 g, 83%). ¹H NMR (CDCl₃): δ 9.27 (s, 1H), 7.76 (s, 1H), 7.57 (d, *J* = 9.0 Hz, 2H), 6.90 (d, *J* = 8.7 Hz, 2H), 5.67 (bs, 1H), 4.30 (q, *J* = 6.9 Hz, 2H), 3.83 (s, 3H), 2.40 (s, 3H), 1.37 (t, *J* = 7.2 Hz, 3H). ¹³C NMR (CDCl₃): δ 165.1, 160.9, 150.3, 149.4, 142.5, 128.3, 126.6, 114.2, 92.5, 59.8, 55.3, 14.5, 14.1. HRMS (*M*⁺): calcd for C₁₅H₁₈N₄O₃, 302.1379; found, 302.1361.

(E)-Ethyl 5-(2-Benzylidenehydrazinyl)-3-methyl-1H-pyrazole-4-carboxylate (8b). Compound **8b** was prepared from **7** and benzaldehyde in 71% yield by the same procedure as described for **8a**. ¹H NMR (CDCl₃): δ 9.40 (s, 1H), 7.78 (s, 1H), 7.57–7.60 (m, 2H), 7.31–7.35 (m, 3H), 4.30 (q, *J* = 7.2 Hz, 2H), 2.39 (s, 3H), 1.36 (t, *J* = 7.2 Hz, 3H). ¹³C NMR (CDCl₃): δ 165.2, 150.5, 148.9, 142.2, 134.0, 129.4, 128.6, 126.7, 92.8, 59.7, 14.4, 13.9. LCMS-ESI (*m/z*): [M + 1]⁺ 273.1, [M + Na]⁺ 295.1.

(E)-3-Methyl-5-(*N'*-phenethylidene-hydrazino)-1H-pyrazole-4-carboxylic Acid Ethyl Ester (8c). Compound **8c** was prepared from **7** and phenylethanal in 41% yield by the same procedure as described for **8a**. ¹H NMR (CDCl₃): δ 9.07 (s, 1H), 7.20–7.37 (m, 6H), 4.26 (q, *J* = 7.2 Hz, 2H), 3.62 (d, *J* = 6.0 Hz, 2H), 2.36 (s, 3H), 1.38 (t, *J* = 7.2 Hz, 3H). LCMS-ESI (*m/z*): [M + 1]⁺ 287.1, [M + Na]⁺ 309.1.

(E)-5-[*N'*-(4-Fluorobenzylidene)hydrazino]-3-methyl-1H-pyrazole-4-carboxylic Acid Ethyl Ester (8d). Compound **8d** was prepared from **7** and 4-fluorobenzaldehyde in 40% yield by the same procedure as described for **8a**. ¹H NMR (CDCl₃): δ 9.39 (s, 1H), 7.79 (s, 1H), 7.59–7.63 (m, 2H), 7.06 (t, 2H), 4.31 (q, *J* = 7.2 Hz, 2H), 2.41 (s, 3H), 1.38 (t, *J* = 7.2 Hz, 3H). LCMS-ESI (*m/z*): [M + 1]⁺ 291.1, [M + Na]⁺ 313.1.

(E)-Ethyl 5-(2-(Biphenyl-4-ylmethylene)hydrazinyl)-3-methyl-1H-pyrazole-4-carboxylate (8e). Compound **8e** was prepared from **7** and 4-biphenylcarboxaldehyde in 42% yield by the same procedure as described for **8a**. ¹H NMR (CDCl₃): δ 9.43 (s, 1H), 7.79 (s, 1H), 7.68 (d, *J* = 8.4 Hz, 2H), 7.56–7.58 (m, 4H), 7.35–7.45 (m, 4H), 5.58 (bs, 2H), 4.30 (q, *J* = 7.1 Hz, 2H), 2.47 (s, 3H), 1.35 (t, *J* = 7.2 Hz, 3H). LCMS-ESI (*m/z*): [M + 1]⁺ 349.2.

(E)-Ethyl 3-Methyl-5-(2-(4-(4-methylpiperazin-1-yl)-benzylidene)hydrazinyl)-1H-pyrazole-4-carboxylate (8f). Compound **8f** was prepared from **7** and 4-(4-methylpiperazin-1-yl)benzaldehyde in 51% yield by the same procedure as described for **8a**. ¹H NMR (CDCl₃): δ 9.22 (s, 1H), 7.71 (s, 1H), 7.49 (d, *J* = 8.7 Hz, 2H), 6.85 (d, *J* = 8.7 Hz, 2H), 4.28 (q, *J* = 7.2 Hz, 2H),

3.26 (t, $J = 4.9$ Hz, 4H), 2.56 (t, $J = 4.9$ Hz, 4H), 2.38 (s, 3H), 2.34 (s, 3H), 1.35 (t, $J = 7.2$ Hz, 3H). LCMS-ESI (m/z): $[M + 1]^+$ 371.2.

(E)-Ethyl 5-(2-((1H-Indol-5-yl)methylene)hydrazinyl)-3-methyl-1H-pyrazole-4-carboxylate (8g). Compound **8g** was prepared from **7** and indole-5-carboxaldehyde in 47% yield by the same procedure as described for **8a**. ^1H NMR (CDCl_3): δ 9.22 (s, 1H), 8.84 (s, 1H), 7.80 (s, 1H), 7.70 (s, 1H), 7.53 (d, $J = 8.7$ Hz, 1H), 7.30 (d, $J = 8.7$ Hz, 1H), 7.17 (s, 1H), 7.00 (br, 1H), 6.50 (s, 1H), 4.29 (q, $J = 7.1$ Hz, 2H), 2.38 (s, 3H), 1.34 (t, $J = 7.1$ Hz, 3H). LCMS-ESI (m/z): $[M + 1]^+$ 312.2, $[2M + \text{Na}]^+$ 645.3.

(E)-Ethyl 5-(2-((1H-Indol-4-yl)methylene)hydrazinyl)-3-methyl-1H-pyrazole-4-carboxylate (8h). Compound **8h** was prepared from **7** and indole-4-carboxaldehyde in 73% yield by the same procedure as described for **8a**. ^1H NMR ($\text{DMSO}-d_6$): δ 11.26 (s, 1H), 9.86 (bs, 1H), 8.57 (s, 1H), 7.37–7.43 (m, 3H), 7.10–7.14 (m, 2H), 4.24 (q, $J = 5.3$ Hz, 2H), 2.30 (s, 3H), 1.31 (t, $J = 5.3$ Hz, 3H). LCMS-ESI (m/z): $[M + 1]^+$ 312.1, $[2M + \text{Na}]^+$ 645.3.

(E)-Ethyl 5-(2-(1-(4-Methoxyphenyl)ethylidene)hydrazinyl)-3-methyl-1H-pyrazole-4-carboxylate (8i). Compound **8i** was prepared from **7** and 4'-methoxyacetophenone in 61% yield by the same procedure as described for **8a**. ^1H NMR (CDCl_3): δ 9.14 (s, 1H), 7.66 (d, $J = 8.7$ Hz, 2H), 6.87 (d, $J = 8.7$ Hz, 2H), 4.30 (q, $J = 6.9$ Hz, 2H), 3.82 (s, 3H), 2.39 (s, 3H), 2.24 (s, 3H), 1.38 (t, $J = 7.2$ Hz, 3H). LCMS-ESI (m/z): $[M + 1]^+$ 317.1.

(E)-5-(2-(4-Methoxybenzylidene)hydrazinyl)-3-methyl-1H-pyrazole-4-carboxylic Acid (10). To a solution of **7** (1.84 g, 10.0 mmol) in 20 mL of water, a solution of aqueous NaOH (0.8 g, 20 mmol, in 20 mL of water) was added, and the reaction mixture was heated at 90 °C for 2 h. The reaction mixture was cooled on an ice bath and neutralized to pH ~7.0 by adding dropwise 2 N HCl. A solution of *p*-anisaldehyde (2.04 g, 15.0 mmol) in EtOAc (10 mL) was added to the aqueous reaction mixture and the reaction mixture heated to 90 °C for 1 h. A yellow-white precipitate of the product had started floating by this time. After the reaction mixture was cooled to room temperature, it was filtered, and the solid product obtained was suspended in EtOAc (10 mL), sonicated, and then filtered. Sonication with EtOAc and filtration was carried out two more times to remove impurities. The residue was dried under vacuum to give pure off-white amorphous powder of **10** (1.51 g, 55%). ^1H NMR ($\text{DMSO}-d_6$): δ 12.14 (bs, 2H), 9.84 (s, 1H), 8.19 (s, 1H), 7.68 (d, $J = 8.4$ Hz, 2H), 6.96 (d, $J = 8.4$ Hz, 2H), 3.79 (s, 3H), 2.26 (s, 3H). ^{13}C NMR ($\text{DMSO}-d_6$): δ 165.4, 160.0, 149.9, 147.6, 142.0, 128.1, 127.7, 114.1, 92.2, 55.2, 13.8. LCMS-ESI (m/z): $[M + 1]^+$ 275.1, $[M + \text{Na}]^+$ 297.1, $[2M + \text{Na}]^+$ 571.2.

(E)-Benzyl 5-(2-(4-Methoxybenzylidene)hydrazinyl)-3-methyl-1H-pyrazole-4-carboxylate (12a). Compound **10** (0.055 g, 0.20 mmol), *N*-hydroxybenzotriazole monohydrate (0.034 g, 0.22 mmol), and 1-(3-dimethylaminopropyl)-3-ethylcarbodiimide hydrochloride (0.042 g, 0.22 mmol) were dissolved in anhydrous DMF (4.0 mL) and stirred for 1 h under nitrogen atmosphere at room temperature. Then benzyl alcohol (0.3 mmol) was added and the reaction mixture was stirred further for 24 h at room temperature. DMF was removed under reduced pressure on a rotary evaporator, and the residue obtained was subjected to preparative TLC by developing the plate twice in a mixture of $\text{CH}_2\text{Cl}_2/\text{MeOH}$ (96:4) to give **12a** (0.019 g, 26%). ^1H NMR (CDCl_3): δ 9.23 (s, 1H), 7.72 (s, 1H), 7.57 (d, $J = 8.7$ Hz, 2H), 7.34–7.44 (m, 5H), 6.91 (d, $J = 8.7$ Hz, 2H), 5.31 (s, 2H), 3.84 (s, 3H), 2.41 (s, 3H). ^{13}C NMR (CDCl_3): δ 164.9, 161.2, 150.6, 149.8, 143.1, 136.6, 128.9, 128.6, 128.4, 128.1, 126.7, 114.4, 92.4, 65.9, 55.6, 14.5. HRMS (M^+): calcd for $\text{C}_{20}\text{H}_{20}\text{N}_4\text{O}_3$, 364.1535; found, 363.1539.

(E)-N-Benzyl-5-(2-(4-methoxybenzylidene)hydrazinyl)-3-methyl-1H-pyrazole-4-carboxamide (12b). Compound **12b** was prepared from **10** and benzylamine in 26% yield by the same procedure as described for **12a**. ^1H NMR (CDCl_3): δ 9.85 (s, 1H), 7.74 (s, 1H), 7.54 (d, $J = 9.0$ Hz, 2H), 7.38–7.28 (m, 5H), 6.88 (d, $J = 9.0$ Hz, 2H), 6.03 (br, 1H), 4.61 (d, $J = 5.4$ Hz, 2H), 3.82 (s, 3H), 2.41 (s, 3H). HRMS (M^+): calcd for $\text{C}_{20}\text{H}_{21}\text{N}_5\text{O}_2$, 363.1695; found, 363.1683.

(E)-5-(2-(4-Methoxybenzylidene)hydrazinyl)-3-methyl-N-phenethyl-1H-pyrazole-4-carboxamide (12c). Compound **12c** was prepared from **10** and phenylethylamine in 23% yield by the same procedure as described for **12a**. ^1H NMR (CDCl_3): δ 9.87 (s, 1H), 7.75 (s, 1H), 7.55 (d, $J = 8.7$ Hz, 2H), 7.36–7.31 (m, 2H), 7.27–7.22 (m, 3H), 6.90 (d, $J = 9.0$ Hz, 2H), 5.58 (br, 1H), 3.83 (s, 3H), 3.68 (q, $J = 6.9$ Hz, 2H), 2.90 (t, $J = 6.9$ Hz, 2H), 2.17 (s, 3H). HRMS (M^+): calcd for $\text{C}_{21}\text{H}_{23}\text{N}_5\text{O}_2$, 377.1852; found, 377.1832.

(E)-5-(2-(4-Methoxybenzylidene)hydrazinyl)-3-methyl-N-(3-phenylpropyl)-1H-pyrazole-4-carboxamide (12d). Compound **12d** was prepared from **10** and phenylpropylamine in 24% yield by the same procedure as described for **12a**. ^1H NMR (CDCl_3): δ 9.85 (s, 1H), 7.74 (s, 1H), 7.54 (d, $J = 8.7$ Hz, 2H), 7.31–7.24 (m, 2H), 7.21–7.15 (m, 3H), 6.89 (d, $J = 9.0$ Hz, 2H), 5.66 (br, 1H), 3.82 (s, 3H), 3.44 (q, $J = 7.2$ Hz, 2H), 2.71 (t, $J = 7.7$ Hz, 2H), 2.36 (s, 3H), 1.94 (p, $J = 7.2$ Hz, 2H). HRMS (M^+): calcd for $\text{C}_{22}\text{H}_{25}\text{N}_5\text{O}_2$, 391.2008; found, 391.1986.

(E)-5-(2-(4-Methoxybenzylidene)hydrazinyl)-3-methyl-N-phenyl-1H-pyrazole-4-carboxamide (12e). Compound **12e** was prepared from **10** and aniline in 15% yield by the same procedure as described for **12a**. ^1H NMR (CDCl_3): δ 9.85 (s, 1H), 7.74 (s, 1H), 7.54 (d, $J = 8.7$ Hz, 2H), 7.31–7.24 (m, 2H), 7.21–7.15 (m, 3H), 6.89 (d, $J = 9.0$ Hz, 2H), 5.66 (br, 1H), 3.82 (s, 3H), 3.44 (q, $J = 7.2$ Hz, 2H), 2.71 (t, $J = 7.7$ Hz, 2H), 2.36 (s, 3H), 1.94 (p, $J = 7.2$ Hz, 2H). HRMS (M^+): calcd for $\text{C}_{19}\text{H}_{19}\text{N}_5\text{O}_2$, 349.1539; found, 349.1522.

(E)-5-(2-(4-Methoxybenzylidene)hydrazinyl)-N,3-dimethyl-N-phenyl-1H-pyrazole-4-carboxamide (12f). Compound **12f** was prepared from **10** and *N*-methylaniline in 17% yield by the same procedure as described for **12a**. ^1H NMR (CDCl_3): δ 9.20 (s, 1H), 7.76 (s, 1H), 7.57 (d, $J = 8.7$ Hz, 2H), 7.31–7.26 (m, 2H), 7.18–7.13 (m, 3H), 6.91 (d, $J = 9.0$ Hz, 2H), 3.84 (s, 3H), 3.46 (s, 3H), 1.46 (s, 3H). LCMS-ESI (m/z): $[M + 1]^+$ 364.2, $[M + \text{Na}]^+$ 386.2.

(E)-N-Benzyl-5-(2-(4-methoxybenzylidene)hydrazinyl)-N,3-dimethyl-1H-pyrazole-4-carboxamide (12g). Compound **12g** was prepared from **10** and *N*-methylbenzylamine in 25% yield by the same procedure as described for **12a**. ^1H NMR (CDCl_3): δ 8.94 (s, 1H), 7.72 (s, 1H), 7.49 (d, $J = 8.4$ Hz, 2H), 7.20–7.33 (m, 5H), 6.83 (d, $J = 8.4$ Hz, 2H), 4.63 (s, 2H), 3.78 (s, 3H), 2.92 (s, 3H), 2.24 (s, 3H). LCMS-ESI (m/z): $[M + 1]^+$ 378.2, $[M + \text{Na}]^+$ 400.2.

(E)-5-(2-(4-Methoxybenzylidene)hydrazinyl)-3-methyl-N-(2-(pyridin-3-yl)ethyl)-1H-pyrazole-4-carboxamide (12h). Compound **12h** was prepared from **10** and 3-(2-aminoethyl)pyridine in 23% yield by the same procedure as described for **12a**. ^1H NMR (CDCl_3): δ 9.80 (s, 1H), 8.50–8.52 (m, 2H), 7.76 (s, 1H), 7.52–7.59 (m, 3H), 7.23–7.28 (m, 1H), 6.90 (d, $J = 8.7$ Hz, 2H), 5.68 (bs, 1H), 3.83 (s, 3H), 3.67 (q, $J = 6.9$ Hz, 2H), 2.92 (t, $J = 6.9$ Hz, 2H), 2.27 (s, 3H). LCMS-ESI (m/z): $[M + 1]^+$ 379.3.

(E)-N-(2-(1H-Imidazol-4-yl)ethyl)-5-(2-(4-methoxybenzylidene)hydrazinyl)-3-methyl-1H-pyrazole-4-carboxamide (12i). Compound **12i** was prepared from **10** and histamine in 15% yield by the same procedure as described for **12a**. ^1H NMR (CDCl_3): δ 10.16 (bs, 1H), 8.10 (s, 1H), 7.69 (d, $J = 8.7$ Hz, 2H), 7.65 (s, 1H), 7.16 (bs, 1H), 6.93–6.98 (m, 3H), 3.83 (s, 3H), 3.60 (q, $J = 6.6$ Hz, 2H), 2.83 (t, $J = 6.6$ Hz, 2H), 2.40 (s, 3H). LCMS-ESI (m/z): $[M + 1]^+$ 368.2, $[M + \text{Na}]^+$ 390.1.

(E)-N-(2-(1H-Indol-3-yl)ethyl)-5-(2-(4-methoxybenzylidene)hydrazinyl)-3-methyl-1H-pyrazole-4-carboxamide (12j). Compound **12j** was prepared from **10** and tryptamine in 20% yield by the same procedure as described for **12a**. ^1H NMR (CDCl_3): δ 9.87 (bs, 1H), 8.47 (s, 1H), 7.61–7.62 (m, 2H), 7.48 (d, $J = 8.7$ Hz, 2H), 7.38 (d, $J = 7.8$ Hz, 1H), 7.09–7.23 (m, 2H), 7.05 (d, $J = 1.8$ Hz, 1H), 6.84 (d, $J = 8.7$ Hz, 2H), 5.76 (t, $J = 4.7$ Hz, 1H), 3.70–3.79 (m, 5H), 3.06 (t, $J = 6.5$ Hz, 2H), 2.05 (s, 3H). LCMS-ESI (m/z): $[M + 1]^+$ 417.2, $[M + \text{Na}]^+$ 439.2.

(E)-N-(4-Methoxybenzyl)-5-(2-(4-methoxybenzylidene)hydrazinyl)-3-methyl-1H-pyrazole-4-carboxamide (12k). Compound **12k** was prepared from **10** and 4-methoxybenzylamine in 25% yield by the same procedure as described for **12a**. ^1H NMR

(CDCl₃): δ 9.85 (s, 1H), 7.75 (s, 1H), 7.55 (d, J = 8.7 Hz, 2H), 7.26 (d, J = 8.4 Hz, 2H), 6.87–6.91 (m, 4H), 5.93 (bs, 1H), 4.54 (d, J = 5.7 Hz, 2H), 3.83 (s, 3H), 3.80 (s, 3H), 2.39 (s, 3H). LCMS-ESI (m/z): [M + 1]⁺ 394.2, [M + Na]⁺ 416.1.

(*E*)-*N*-(3-Methoxybenzyl)-5-(2-(4-methoxybenzylidene)hydrazinyl)-3-methyl-1*H*-pyrazole-4-carboxamide (12l). Compound **12l** was prepared from **10** and 3-methoxybenzylamine in 25% yield by the same procedure as described for **12a**. ¹H NMR (CDCl₃): δ 9.85 (s, 1H), 7.76 (s, 1H), 7.56 (d, J = 9.0 Hz, 2H), 7.25–7.30 (m, 2H), 6.81–6.94 (m, 4H), 5.95 (bs, 1H), 4.59 (d, J = 5.7 Hz, 2H), 3.84 (s, 3H), 3.80 (s, 3H), 2.42 (s, 3H). LCMS-ESI (m/z): [M + 1]⁺ 394.0.

(*E*)-*N*-(3-Acetamidobenzyl)-5-(2-(4-methoxybenzylidene)hydrazinyl)-3-methyl-1*H*-pyrazole-4-carboxamide (12m). Compound **12m** was prepared from **10** and 3-acetamidobenzylamine in 15% yield by the same procedure as described for **12a**. ¹H NMR (CDCl₃ + CD₃OD): δ 7.72 (s, 1H), 7.44–7.55 (m, 4H), 7.23 (d, J = 8.1 Hz, 1H), 7.01 (d, J = 7.5 Hz, 1H), 6.86 (d, J = 9.0 Hz, 2H), 4.51 (s, 2H), 3.80 (s, 3H), 2.42 (s, 3H), 2.10 (s, 3H). LCMS-ESI (m/z): [M + 1]⁺ 421.2, [M + Na]⁺ 443.1.

(*E*)-5-(2-(4-Methoxybenzylidene)hydrazinyl)-*N*-(4-methoxyphenethyl)-3-methyl-1*H*-pyrazole-4-carboxamide (12n). Compound **12n** was prepared from **10** and 4-methoxyphenethylamine in 22% yield by the same procedure as described for **12a**. ¹H NMR (CDCl₃): δ 9.87 (s, 1H), 7.74 (s, 1H), 7.53 (d, J = 8.4 Hz, 2H), 7.14 (d, J = 8.4 Hz, 2H), 6.84–6.89 (m, 4H), 5.61 (bs, 1H), 3.82 (s, 3H), 3.79 (s, 3H), 3.64 (q, J = 6.8 Hz, 2H), 2.83 (t, J = 6.8 Hz, 2H), 2.20 (s, 3H). LCMS-ESI (m/z): [M + 1]⁺ 408.2.

(*E*)-5-(2-(4-Methoxybenzylidene)hydrazinyl)-*N*-(3-methoxyphenethyl)-3-methyl-1*H*-pyrazole-4-carboxamide (12o). Compound **12o** was prepared from **10** and 3-methoxyphenethylamine in 24% yield by the same procedure as described for **12a**. ¹H NMR (CDCl₃): δ 9.87 (s, 1H), 7.75 (s, 1H), 7.54 (d, J = 8.7 Hz, 2H), 7.24 (td, J = 7.2, 1.2 Hz, 1H), 6.89 (d, J = 8.7 Hz, 2H), 6.77–6.83 (m, 3H), 5.62 (bs, 1H), 3.83 (s, 3H), 3.79 (s, 3H), 3.67 (q, J = 6.9 Hz, 2H), 2.87 (t, J = 6.5 Hz, 2H), 2.19 (s, 3H). LCMS-ESI (m/z): [M + 1]⁺ 408.2.

(*E*)-5-(2-(4-Methoxybenzylidene)hydrazinyl)-*N*-(4-methoxyphenyl)-3-methyl-1*H*-pyrazole-4-carboxamide (12p). Compound **12p** was prepared from **10** and 4-methoxyaniline in 17% yield by the same procedure as described for **12a**. ¹H NMR (CDCl₃): δ 9.81 (s, 1H), 7.76 (s, 1H), 7.57 (d, J = 8.7 Hz, 2H), 7.42 (d, J = 8.7 Hz, 2H), 7.38 (bs, 1H), 6.89–6.93 (m, 4H), 3.84 (s, 3H), 3.81 (s, 3H), 2.56 (s, 3H). HRMS (M^+): calcd for C₂₀H₂₁N₅O₃, 379.1644; found, 379.1646.

(*E*)-5-(2-(4-Methoxybenzylidene)hydrazinyl)-*N*-(3-methoxyphenyl)-3-methyl-1*H*-pyrazole-4-carboxamide (12q). Compound **12q** was prepared from **10** and 3-methoxyaniline in 17% yield by the same procedure as described for **12a**. ¹H NMR (CDCl₃): δ 9.78 (bs, 1H), 7.78 (s, 1H), 7.56 (d, J = 8.7 Hz, 2H), 7.28 (t, J = 2.1 Hz, 1H), 7.23 (d, J = 8.1 Hz, 1H), 7.01 (dd, J = 7.8, 2.1 Hz, 1H), 6.90 (d, J = 8.7 Hz, 2H), 6.68 (d, J = 8.1 Hz, 1H), 3.83 (s, 3H), 3.82 (s, 3H), 2.56 (s, 3H). HRMS (M^+): calcd for C₂₀H₂₁N₅O₃, 379.1644; found, 379.1650.

(*E*)-5-(2-(4-Methoxybenzylidene)hydrazinyl)-*N*-(2-methoxyphenyl)-3-methyl-1*H*-pyrazole-4-carboxamide (12r). Compound **12r** was prepared from **10** and 2-methoxyaniline in 15% yield by the same procedure as described for **12a**. ¹H NMR (CDCl₃): δ 9.96 (s, 1H), 8.42 (dd, J = 7.5, 2.0 Hz, 1H), 8.18 (s, 1H), 7.79 (s, 1H), 7.56 (d, J = 8.1 Hz, 2H), 6.97–7.26 (m, 2H), 6.88–6.93 (m, 3H), 3.92 (s, 3H), 3.82 (s, 3H), 2.58 (s, 3H). HRMS (M^+): calcd for C₂₀H₂₁N₅O₃, 379.1644; found, 379.1641.

(*E*)-*N*-(3,4-Dimethoxyphenyl)-5-(2-(4-methoxybenzylidene)hydrazinyl)-3-methyl-1*H*-pyrazole-4-carboxamide (12s). Compound **12s** was prepared from **10** and 3,4-dimethoxyaniline in 17% yield by the same procedure as described for **12a**. ¹H NMR (CDCl₃): δ 9.74 (s, 1H), 7.78 (s, 1H), 7.56 (d, J = 8.4 Hz, 2H), 7.50 (bs, 1H), 7.30 (d, J = 2.4 Hz, 1H), 6.88–6.93 (m, 3H), 6.84 (d, J = 9.0 Hz, 1H), 3.90 (s, 3H), 3.88 (s, 3H), 3.83 (s, 3H), 2.57 (s, 3H). LCMS-ESI (m/z): [M + 1]⁺ 410.1.

(*E*)-*N*-(4-(Dimethylamino)phenyl)-5-(2-(4-methoxybenzylidene)hydrazinyl)-3-methyl-1*H*-pyrazole-4-carboxamide (12t). Compound **12t** was prepared from **10** and *N,N*-dimethylaniline in 17% yield by the same procedure as described for **12a**. ¹H NMR (CDCl₃): δ 9.88 (s, 1H), 7.76 (s, 1H), 7.58 (d, J = 8.7 Hz, 2H), 7.35 (d, J = 8.7 Hz, 2H), 6.92 (d, J = 9.0 Hz, 2H), 6.75 (d, J = 9.0 Hz, 2H), 3.84 (s, 3H), 2.94 (s, 6H), 2.55 (s, 3H). LCMS-ESI (m/z): [M + 1]⁺ 393.1, [M + Na]⁺ 415.2.

(*E*)-*N*-(4-Fluorophenyl)-5-(2-(4-methoxybenzylidene)hydrazinyl)-3-methyl-1*H*-pyrazole-4-carboxamide (12u). Compound **12u** was prepared from **10** and 4-fluoroaniline in 15% yield by the same procedure as described for **12a**. ¹H NMR (CDCl₃): δ 9.70–9.98 (br, 1H), 7.79 (s, 1H), 7.58 (d, J = 8.7 Hz, 2H), 7.46–7.51 (m, 2H), 7.06 (t, J = 8.7 Hz, 2H), 6.92 (d, J = 8.7 Hz, 2H), 3.85 (s, 3H), 2.57 (s, 3H). LCMS-ESI (m/z): [M + 1]⁺ 368.1, [M + Na]⁺ 390.1.

(*E*)-*N*-(4-Acetamidophenyl)-5-(2-(4-methoxybenzylidene)hydrazinyl)-3-methyl-1*H*-pyrazole-4-carboxamide (12v). Compound **12v** was prepared from **10** and 4-acetamidophenylamine in 15% yield by the same procedure as described for **12a**. ¹H NMR (CDCl₃ + CD₃OD): δ 7.82 (s, 1H), 7.58 (d, J = 8.7 Hz, 2H), 7.37–7.47 (m, 4H), 6.86 (d, J = 9.0 Hz, 2H), 3.78 (s, 3H), 2.57 (s, 3H), 2.08 (s, 3H). HRMS (M^+): calcd for C₂₁H₂₂N₆O₃, 406.1753; found, 406.1756.

(*E*)-*N*-(3-Acetamidophenyl)-5-(2-(4-methoxybenzylidene)hydrazinyl)-3-methyl-1*H*-pyrazole-4-carboxamide (12w). Compound **12w** was prepared from **10** and 3-acetamidophenylamine in 15% yield by the same procedure as described for **12a**. ¹H NMR (CDCl₃ + CD₃OD): δ 7.72–7.74 (m, 2H), 7.54 (d, J = 8.7 Hz, 2H), 7.33 (d, J = 7.5 Hz, 1H), 7.12–7.23 (m, 2H), 6.86 (d, J = 9.0 Hz, 2H), 3.79 (s, 3H), 2.48 (s, 3H), 2.10 (s, 3H). ¹³C NMR (CDCl₃): δ 168.3, 163.2, 160.9, 150.3, 145.3, 142.7, 138.5, 138.4, 129.6, 128.3, 126.6, 115.9, 115.3, 114.2, 111.5, 55.4, 24.7, 15.0. HRMS (M^+): calcd for C₂₁H₂₂N₆O₃, 406.1753; found, 406.1755.

Virtual Screening. The GOLD program (version 3.1) was applied to screen 59 488 molecules from Maybridge database (Tintagel, Cornwall, England). The crystal structure of Aurora kinase A in complex with ADP (PDB ID 1OL5) was used as the template for docking. Residues within a radius of 15 Å centered on CA atom of Glu211 were defined as the active site. Twenty genetic algorithm (GA) runs were performed for each molecule. For each GA run, 100 000 operations were applied on a set of five islands with a population size of 100. The weights for three types of operations (crossover, mutation, and migration) were chosen as 95%, 95%, and 10%, respectively. The selection pressure, which is the ratio between the probability of the most fit member selected as a parent to the probability of an average member selected as a parent, was set at 1:1. The annealing parameters of van der Waals and hydrogen bonding were set at 4.0 and 2.5 Å to allow a few bad bumps and poor hydrogen bonds at the beginning of a GA run. The “early-termination” option was turned off to allow the continued docking even though the first three docking solutions were very similar, with the root-mean-square deviation (rmsd) less than 1.5 Å. Moreover, analysis of various Aurora kinase–inhibitor complex structures revealed important hydrogen bonding interactions with Glu211 and Ala213. Therefore, hydrogen bond constraints with a constraint weight of 10 were applied to specify that Glu211 and/or Ala213 should form the H-bond with the docked compounds. Absence of the hydrogen bonding interactions with either Glu211 or Ala213 was penalized by the value of 10 in the GoldScore function. GoldScore implemented in GOLD was applied to rank the docked compounds.

Expression and Purification of Aurora A. Aurora A catalytic domain (residues 123–401), with one mutation at residue 288 (T288D) and six His as the tag at the N-terminus, was cloned into the pET-28a vector and expressed in BL21 DE3 *E. coli*. The protein was then purified by nickel column following the procedures suggested by the suppliers (Amersham Biosciences, Piscataway, NJ). The bound protein was washed with 10% of buffer solution (40 mmol HEPES (pH 7.5), 50 mmol NaCl, and 500 mmol imidazole) and eluted with 100% of buffer solution. The fractions

containing Aurora A catalytic domain were then treated with TEV protease (Invitrogen) overnight at 4 °C to remove the His tag and concentrated to 8 mg/mL in a buffer containing 40 mmol of HEPES, pH 7.5, 50 mmol NaCl, 1 mmol DTT.

Crystallization and Structure Determination. The hanging drop method was used to obtain the crystals of Aurora A in complex with the compounds. A drop of 1.5 μ L of protein preincubated with the compound for a half-hour on ice was mixed with an equal volume of reservoir solution (22% PEG400 and 0.1 mmol of ammonia sulfate). The crystals were grown at 18 °C for 3–7 days. Before being flash-frozen in liquid nitrogen, the crystal was immersed briefly in a cryoprotectant containing 37% PEG400. Diffraction data were collected on beamline SP12B2 at the Spring-8 (Japan) and beamlines BL13B1 and BL13C1 at the NSRR (Taiwan). The data were processed by DENZO²² and reduced with SCALEPACK. The structure was solved by molecular replacement in MOLREP²³ using the published Aurora A structure (PDB ID 1MQ4) as the search model. The refinement calculations were performed by REFMAC5,²⁴ and model building was carried out with the program O9.0.²⁵ The coordinates of the aurora A/compound **12w** have been deposited in the Protein Data Bank with accession code “3FDN”.

Determination of Phospho Histone H3 (Ser10) and Phospho Aurora A (Thr288) Suppression in HCT-116 Tumor Cells by Western Blotting Analysis. HCT-116 cells (4×10^5) were seeded in each well of a six-well plate for 24 h in culture medium, followed by synchronization with 40 ng/mL nocodazole for 16 h. Then the cells were exposed to various concentrations of test compound (40, 20, 10, 5, 2.5, 1.25, 0.625 μ M for **12w** and 0.25 μ M for **1**) at 37 °C for 2 h. Cells were harvested by washing twice with cold PBS and lysed in 128 μ L of 1 \times SDS sample buffer (125 mmol/L Tris-HCl, pH 6.8, and 2% SDS). After addition of SDS sample buffer, the lysate was heated at 95 °C for 10 min and an amount of 50 μ g of samples was redissolved by 10% or 15% SDS–polyacrylamide gel electrophoresis and then transferred to a nitrocellular membrane (BioTrace). After transfer, the membrane was incubated in TBST buffer (20 mmol Tris, pH 7.5, 136 mmol NaCl, and 0.1% (v/v) Tween-20) with 5% (w/v) milk powder and then incubated with the indicated primary antibody (dilution of antibodies was performed according to the manufacturer's instructions), washed, and blotted with horseradish peroxidase conjugated secondary antibody. Immunodetection was done using the following primary antibodies: anti-histone H3 (Cell Signaling), anti-Ser10P-histone H3 (Cell Signaling), anti-Aurora A (Abcam), anti-Thr288P-Aurora A (Cell Signaling), and anti- γ -tubulin (Sigma). The membrane was then developed using Super-Signal reagent (Pierce) and exposed to X-ray film.

Acknowledgment. We thank the staff at beamline BL13B1 and BL13C1 at National Synchrotron Radiation Research Centre (NSRR), Taiwan, and the staff at beamline SP12B2 at Spring-8, Japan, for technical assistance. Also, we thank Mark Swofford for helping with the English editing. The authors acknowledge the financial support by National Science Council, Taiwan (Grant Nos. NSC-96-2113-M-400-001-MY3 for S.-Y.W; NSC-95-2113-M-400-001-MY3 and NSC-95-2752-B-007-002-PAE for H.-P.H).

Supporting Information Available: X-ray refinement statistics for **8a** and **12a–e,w**; HPLC purity data for **8a,b,d,f,g–i** and **12a–c,e,j,n,p,q,w**. This material is available free of charge via the Internet at <http://pubs.acs.org>.

References

- (1) Fu, J.; Bian, M.; Jiang, Q.; Zhang, C. Roles of Aurora kinases in mitosis and tumorigenesis. *Mol. Cancer Res.* **2007**, *5*, 1–10.
- (2) Carmena, M.; Earnshaw, W. C. The cellular geography of aurora kinases. *Nat. Rev. Mol. Cell Biol.* **2003**, *4*, 842–854.
- (3) Agnese, V.; Bazan, V.; Fiorentino, F. P.; Fanale, D.; Badalamenti, G.; Colucci, G.; Adamo, V.; Santini, D.; Russo, A. The role of Aurora-A inhibitors in cancer therapy. *Ann. Oncol.* **2007**, *18* (Suppl. 6), vi47–vi52.
- (4) Cheetham, G. M.; Charlton, P. A.; Golec, J. M.; Pollard, J. R. Structural basis for potent inhibition of the Aurora kinases and a T315I multi-drug resistant mutant form of Abl kinase by VX-680. *Cancer Lett.* **2007**, *251*, 323–329.
- (5) Harrington, E. A.; Bebbington, D.; Moore, J.; Rasmussen, R. K.; Ajose-Adeogun, A. O.; Nakayama, T.; Graham, J. A.; Demur, C.; Hercend, T.; Diu-Hercend, A.; Su, M.; Golec, J. M.; Miller, K. M. VX-680, a potent and selective small-molecule inhibitor of the Aurora kinases, suppresses tumor growth in vivo. *Nat. Med.* **2004**, *10*, 262–267.
- (6) Fancelli, D.; Moll, J.; Varasi, M.; Bravo, R.; Artico, R.; Berta, D.; Bindi, S.; Cameron, A.; Candiani, I.; Cappella, P.; Carpinelli, P.; Croci, W.; Forte, B.; Giorgini, M. L.; Klapwijk, J.; Marsiglio, A.; Pesenti, E.; Rocchetti, M.; Roletto, F.; Severino, D.; Soncini, C.; Storici, P.; Tonani, R.; Zugnoni, P.; Vianello, P. 1,4,5,6-Tetrahydropyrrolo[3,4-c]pyrazoles: identification of a potent Aurora kinase inhibitor with a favorable antitumor kinase inhibition profile. *J. Med. Chem.* **2006**, *49*, 7247–7251.
- (7) Carpinelli, P.; Ceruti, R.; Giorgini, M. L.; Cappella, P.; Gianellini, L.; Croci, V.; Degraffi, A.; Texido, G.; Rocchetti, M.; Vianello, P.; Rusconi, L.; Storici, P.; Zugnoni, P.; Arrigoni, C.; Soncini, C.; Alli, C.; Patton, V.; Marsiglio, A.; Ballinari, D.; Pesenti, E.; Fancelli, D.; Moll, J. PHA-739358, a potent inhibitor of Aurora kinases with a selective target inhibition profile relevant to cancer. *Mol. Cancer Ther.* **2007**, *6*, 3158–3168.
- (8) Manfredi, M. G.; Ecsedy, J. A.; Meetze, K. A.; Balani, S. K.; Burenkova, O.; Chen, W.; Galvin, K. M.; Hoar, K. M.; Huck, J. J.; LeRoy, P. J.; Ray, E. T.; Sells, T. B.; Stringer, B.; Stroud, S. G.; Vos, T. J.; Weatherhead, G. S.; Wysong, D. R.; Zhang, M.; Bolen, J. B.; Claiborne, C. F. Antitumor activity of MLN8054, an orally active small-molecule inhibitor of Aurora A kinase. *Proc. Natl. Acad. Sci. U.S.A.* **2007**, *104*, 4106–4111.
- (9) Mortlock, A. A.; Foote, K. M.; Heron, N. M.; Jung, F. H.; Pasquet, G.; Lohmann, J. J.; Warin, N.; Renaud, F.; De Savi, C.; Roberts, N. J.; Johnson, T.; Dousson, C. B.; Hill, G. B.; Perkins, D.; Hatter, G.; Wilkinson, R. W.; Wedge, S. R.; Heaton, S. P.; Odedra, R.; Keen, N. J.; Crafter, C.; Brown, E.; Thompson, K.; Brightwell, S.; Khatri, L.; Brady, M. C.; Kearney, S.; McKillop, D.; Rhead, S.; Parry, T.; Green, S. Discovery, synthesis, and in vivo activity of a new class of pyrazoloquinazolines as selective inhibitors of aurora B kinase. *J. Med. Chem.* **2007**, *50*, 2213–2224.
- (10) Wilkinson, R. W.; Odedra, R.; Heaton, S. P.; Wedge, S. R.; Keen, N. J.; Crafter, C.; Foster, J. R.; Brady, M. C.; Bigley, A.; Brown, E.; Byth, K. F.; Barrass, N. C.; Mundt, K. E.; Foote, K. M.; Heron, N. M.; Jung, F. H.; Mortlock, A. A.; Boyle, F. T.; Green, S. AZD1152, a selective inhibitor of Aurora B kinase, inhibits human tumor xenograft growth by inducing apoptosis. *Clin. Cancer Res.* **2007**, *13*, 3682–3688.
- (11) Liou, J. P.; Chang, Y. L.; Kuo, F. M.; Chang, C. W.; Tseng, H. Y.; Wang, C. C.; Yang, Y. N.; Chang, J. Y.; Lee, S. J.; Hsieh, H. P. Concise synthesis and structure–activity relationships of combretastatin A-4 analogues, 1-aroylindoles and 3-aroylindoles, as novel classes of potent antitubulin agents. *J. Med. Chem.* **2004**, *47*, 4247–4257.
- (12) Heron, N. M.; Anderson, M.; Blowers, D. P.; Breed, J.; Eden, J. M.; Green, S.; Hill, G. B.; Johnson, T.; Jung, F. H.; McMiken, H. J.; Mortlock, A. A.; Pannifer, A. D.; Pauptit, R. A.; Pink, J.; Roberts, N. J.; Rowsell, S. SAR and inhibitor complex structure determination of a novel class of potent and specific Aurora kinase inhibitors. *Bioorg. Med. Chem. Lett.* **2006**, *16*, 1320–1323.
- (13) Warner, S. L.; Bashyam, S.; Vankayalapati, H.; Bearss, D. J.; Han, H.; Mahadevan, D.; Von Hoff, D. D.; Hurley, L. H. Identification of a lead small-molecule inhibitor of the Aurora kinases using a structure-assisted, fragment-based approach. *Mol. Cancer Ther.* **2006**, *5*, 1764–1773.
- (14) Fu, D. H.; Jiang, W.; Zheng, J. T.; Zhao, G. Y.; Li, Y.; Yi, H.; Li, Z. R.; Jiang, J. D.; Yang, K. Q.; Wang, Y.; Si, S. Y. Jadomycin B, an Aurora-B kinase inhibitor discovered through virtual screening. *Mol. Cancer Ther.* **2008**, *7*, 2386–2393.
- (15) Deng, X. Q.; Wang, H. Y.; Zhao, Y. L.; Xiang, M. L.; Jiang, P. D.; Cao, Z. X.; Zheng, Y. Z.; Luo, S. D.; Yu, L. T.; Wei, Y. Q.; Yang, S. Y. Pharmacophore modelling and virtual screening for identification of new Aurora-A kinase inhibitors. *Chem. Biol. Drug Des.* **2008**, *71*, 533–539.
- (16) Tari, L. W.; Hoffman, I. D.; Bensen, D. C.; Hunter, M. J.; Nix, J.; Nelson, K. J.; McRee, D. E.; Swanson, R. V. Structural basis for the inhibition of Aurora A kinase by a novel class of high affinity disubstituted pyrimidine inhibitors. *Bioorg. Med. Chem. Lett.* **2007**, *17*, 688–691.
- (17) Nowakowski, J.; Cronin, C. N.; McRee, D. E.; Knuth, M. W.; Nelson, C. G.; Pavletich, N. P.; Rogers, J.; Sang, B. C.; Scheibe, D. N.;

- Swanson, R. V.; Thompson, D. A. Structures of the cancer-related Aurora-A, FAK, and EphA2 protein kinases from nanovolume crystallography. *Structure* **2002**, *10*, 1659–1667.
- (18) Coumar, M. S.; Wu, J. S.; Leou, J. S.; Tan, U. K.; Chang, C. Y.; Chang, T. Y.; Lin, W. H.; Hsu, J. T.; Chao, Y. S.; Wu, S. Y.; Hsieh, H. P. Aurora kinase A inhibitors: identification, SAR exploration and molecular modeling of 6,7-dihydro-4*H*-pyrazolo-[1,5-*a*]pyrrolo[3,4-*d*]pyrimidine-5,8-dione scaffold. *Bioorg. Med. Chem. Lett.* **2008**, *18*, 1623–1627.
- (19) Bailey, J. Synthesis of 1*H*-pyrazolo[3,2-*c*]-*s*-triazoles and derived azamethine dyes. *J. Chem. Soc., Perkin Trans. 1* **1977**, *18*, 2047–2052.
- (20) Jansma, A.; Zhang, Q.; Li, B.; Ding, Q.; Uno, T.; Bursulaya, B.; Liu, Y.; Furet, P.; Gray, N. S.; Geierstanger, B. H. Verification of a designed intramolecular hydrogen bond in a drug scaffold by nuclear magnetic resonance spectroscopy. *J. Med. Chem.* **2007**, *50*, 5875–5877.
- (21) Carpinelli, P.; Moll, J. Aurora kinase inhibitors: identification and preclinical validation of their biomarkers. *Expert Opin. Ther. Targets* **2008**, *12*, 69–80.
- (22) Otwinowski, Z.; Minor, W. Processing of X-ray diffraction data collected in oscillation mode. *Methods Enzymol.* **1997**, *276*, 307–326.
- (23) Vagin, A.; Teplyakov, A. MOLREP: an automated program for molecular replacement. *J. Appl. Crystallogr.* **1997**, *30*, 1022–1025.
- (24) Murshudov, G. N.; Vagin, A. A.; Dodson, E. J. Refinement of macromolecular structures by the maximum-likelihood method. *Acta Crystallogr. D* **1997**, 240–255.
- (25) Jones, T. A.; Zou, J. Y.; Cowan, S. W.; Kjeldgaard, M. Improved methods for building protein models in electron density maps and the location of errors in these models. *Acta Crystallogr. A* **1991**, 110–119.

JM801270E